Volumetric 23 Na Single and Triple-Quantum Imaging at 7T: 3D-CRISTINA

Michaela A.U. Hoesl, Lothar R Schad, Stanislas Rapacchi

Volumetric ^{23}Na Single and Triple-Quantum Imaging at 7T: 3D-CRISTINA

Michaela AU Hoesl PhD[1], Lothar R Schad PhD[1,*], Stanislas Rapacchi PhD[2,*]

[1] Computer Assisted Clinical Medicine, Heidelberg University, 68167 Mannheim, Germany

2 Aix-Marseille Univ, CNRS, CRMBM, Marseille, France

[*] Author Lothar R Schad and Author Stanislas Rapacchi contributed equally to this work

Corresponding author:

Michaela A U Hoesl, PhD

Computer Assisted Clinical Medicine , Heidelberg University

68167 Mannheim, Germany

Email: michaela.hoesl@gmail.de

Running Title: 3D-CRISTINA Imaging

Word count: 3670 words 7 figures 1 table

ABSTRACT

PURPOSE To measure multi-quantum coherence (MQC) ^{23}Na signals for noninvasive cell physiological information in the whole-brain, the 2D-CRISTINA method was extended to 3D. This experimental study investigated the use and results of a new sequence, 3D-CRISTINA, on a phantom and healthy volunteers.

METHODS: The 3D Cartesian single and triple-quantum imaging of ^{23}Na (3D-CRISTINA) was developed and implemented at 7T, favoring a non-selective volume excitation for increased signal-to-noise ratio (SNR) and lower energy deployment than its 2D counterpart. Two independent phase cycles were used in analogy to the 2D method. A comparison of 6-steps cycles and 12-steps cycles was performed.

We used a phantom composed of different sodium and agarose concentrations, 50 mM to 150 mM Na+, and 0–5 % agarose for sequence validation. Four healthy volunteers were scanned at 7T for whole brain MQC imaging. The sequence 3D-CRISTINA was developed and tested at 7T.

RESULTS: At 7T, the 3D-CRISTINA acquisition allowed to reduce the TR to 230 ms from the previous 390 ms for 2D, resulting in a total acquisition time of 53 min for a 3D volume of 4x4x8 mm resolution. The phase cycle evaluation showed that the 7T acquisition time could be reduced by 4-fold with moderate single and triple-quantum signals SNR loss. The healthy volunteers demonstrated clinical feasibility at 7T and showed a difference in the MQC signals ratio of White Matter (WM) and Grey Matter (GM).

CONCLUSION: Volumetric CRISTINA multi-quantum imaging allowed whole-brain coverage. The non-selective excitation enabled a faster scan due to a decrease in energy deposition which enabled a lower repetition time. Thus, it should be the preferred choice for future in vivo multi-quantum applications compared to the 2D

method. A more extensive study is warranted to explore WM and GM MQC differences.

Keywords: sodium MRI, sodium triple-quantum imaging, whole-brain imaging

1 INTRODUCTION

Recently we proposed a 2D multi-quantum coherence (MQC) imaging method for ^{23}Na at 7T, CRISTINA [1], to fully exploit the potential of the spin 3/2 nuclei.

Sodium MRI is of interest for its noninvasive cell physiological information which are connected to multiple pathologies [2]–[10] and therefore could provide improved tissue characterization. MQC imaging focus lays on the joint measurements of single quantum (SQ) signal, for sodium concentration quantification, and triple quantum (TQ) signal, for information about the direct environment of the sodium nuclei, which differs from microscopic environment density and arises from the mechanism of biexponential relaxation.

The typical MQC three-pulses sequence leverages repetitions with a phase-cycling scheme for each quantum signal to follow different coherence pathways. CRISTINA provided an analytical understanding of phase cycling options, leading to an optimal phase-cycling design for simultaneous measurement of SQ and TQ coherence signals robust to B0 inhomogeneity, compared to the state-of-the-art SISTINA sequence that kept a bias due off-resonance phase accrual. The method consists of 2 × 6 steps phase cycles with a phase-increment of π/6. In the first cycle, the start phase for the first pulse is π/2, and the phase difference between the first and second pulse is also π/2. The second cycle has a start phase of 0 (first pulse) and a phase difference of 0 between the first and second pulse.

The experimental results were limited so far to elongated acquisitions for a single 2D plane [1]. The purpose of this study is to communicate practical benefits from the development of volumetric 3D-CRISTINA for 7T.

So far, the three pulses [11], multi-echo 2D-CRISTINA sequence was lacking a volumetric acquisition, needed for improved resolution, an extended field of view, and partial volume effects reduction to reach towards larger scale in vivo explorations.

Further, the long acquisition times at 7T of up to an hour mainly due to an elongated repetition time (TR) of 390 ms from specific absorption rate (SAR) restrictions, with conservative 12-step sampling and 10-fold averaging for a single slice was too long for multi-slice acquisition. The long TR was needed to reduce the SAR of the sinc-shaped, slice selective excitation.

A barrier of ^{23}Na MRI is the low SNR and resulting long acquisition times which is why the higher field strength of 7T was favoured due to the supralinear rise of SNR with the static magnetic field B0. [12] The purpose of this paper is to present 3D-CRISTINA feasibility at 7T. A phase cycle optimization led to the decrease of the total measurement time from 66 min to 32 min (phantom) and from 53 min to 13 min (in vivo). With 3D-CRISTINA, 3D single and triple quantum Images can be obtained simultaneously, within a reasonable acquisition time at 7T. The time efficiency of 3D-CRISTINA is validated on phantom measurements and MQC images are shown in vivo on four healthy volunteers.

2 MATERIAL AND METHODS

2.1 SEQUENCE DEVELOPMENT

The 2D-CRISTINA sequence [1] (**Figure 1 a**) was modified for the 3D-CRISTINA sequence (**Figure 1 b**) to feature a volumetric, multi-echo acquisition for joint multi-quantum signals and tissue sodium concentration (TSC) characterization. 3D-CRISTINA allows for a non-selective excitation to be employed with 3D Cartesian k-space sampling. CRISTINA used an optimal phase-cycle scheme of 2 x 6 = 12 steps with 1) first pulse start phase of π/2, a phase difference between the first and second pulse of π/2 and 2) first pulse start phase of 0 and phase difference between first and

second pulse also 0 with a phase increment of π/6 was acquired. A detailed description about the underlying theory and choice can be found here: [1].

99 *2.2 EXPERIMENTAL VALIDATION*

100 The sequence was tested on an agarose phantom on a 7T scanner (Siemens
101 Healthcare, Magnetom 2nd generation whole body research system, Erlangen,
102 Germany) with a 1Tx/1Rx dual-tuned $^{1}H/^{23}Na$ birdcage head coil (Rapid, Biomedical).
103 The phantom consisted of 9 tubes (14 and 40 mL) with varying concentrations of
104 agarose (0-5 %) and sodium (50-154 mM) (see **Figure 2 A**).
105 Signal-to-noise ratio (SNR) was evaluated as the mean signal in a region of interest
106 (ROI) covering the brain over the standard deviation of the signal in a background
107 ROI outside of the brain. A correction factor of 0.655 was applied to account for the
108 Rayleigh distribution of background noise. SNR of the two 40 mL tubes with 100 mM
109 of sodium and 4 and 5 % agarose was compared between the 3D-CRISTINA and the
110 2D-CRISTINA images as previously described [1] for each echo time. The SNR was
111 further corrected for the voxel size to evaluate SNR variation associated with 3D
112 excitation.
113 The dataset was further downsampled along the phase cycle dimension to investigate
114 optimal choice for phase cycling options to further reduce acquisition time. Detailed
115 sequence parameters are listed in **Table 1**. The vendor internal shimming procedure
116 was repeated at least three times, carefully checking the frequency offset to be zero
117 before each ^{23}Na scan. An incremental free-induction decay-based B1+ calibration
118 was carried out before each scan to calculate the exact reference voltage for the 90°
119 pulses.
120

3D_CRISTINA PARAMETERS	*Phantom*	*In vivo volunteers (1- 4)*
matrix size	*48x48x14x20x24*	*32x32x12x20x24*
size after zero filling	*256x256x14x20*	*128x128x12x20*
base resolution	*48*	*32*
FOV	*200 mm*	*250mm*
resolution	*4x4x8 mm^3*	*7.8x7.8x15 mm^3*
1st pulse duration	*1800 µs*	*1800*
2nd/3rd pulse duration	*1000 µs*	*1000*
TE_1, ΔTE	*1.6 ms*	*1.6 ms*
TR	*160 ms*	*230 ms*
Bandwidth	*400 Hz/px*	*400 Hz/px*
Phasecycles	*2*	*2*
total scan time	*2x**32.8 min** = 66 min*	*2x26.7 min= 53 min*
xRef Voltage	*406 V*	*438 V, 452 V, 415 V, 437 V*

Table 1: 3D Sequence Parameters at 7T. In vivo, the TR varied from the first to the second volunteer due to a higher reference voltage and SAR restriction. The TR was fixed to a higher parameter for the latter two volunteers. Further parameters which did not change between phantom and in vivo scans were: ($\Delta\phi = 30°$) resulting in a phase cycle of 12 points, mixing time = 100 µs, evolution time = 10 ms, number of echoes = 20, asymmetry of echo = 0.8. Slice thickness 3D = 15 mm (in vivo), 8 mm (phantom).

2.3 IN VIVO VALIDATION

Four healthy volunteers (1 woman, 3 men, 21±0.5 years old) were recruited after providing informed consent according to the Declaration of Helsinki. The study was approved by the local ethical committee. Four additional 60 mL phantom vials were placed next to the head for sodium quantification, containing 5% and 2% agarose each with 100 mM and 50 mM Na+ concentration. The phantoms were fixed to the subjects' head with an elastic band. Additionally, to achieve TSC quantification the cerebrospinal fluid (CSF) Na^+ literature value of 145 mM was used [13]. For one healthy volunteer we retrospectively undersampled the data to virtually reduce the measurement time according to the phantom 7T data.

2.4 DATA RECONSTRUCTION AND FIT

In analogy to the data reconstruction for the 2D-CRISTINA sequence, the reconstruction was extended to 3D including the additional slice dimension. A 3D B0 map was calculated from the first two echoes of the CRISTINA phase data to map the signal off-resonances for combination of the two phase cycles ($\xi_1 = \pi/2 \; and \; \xi_2 = 0$) according to the method of *Fleysher et al*.[14] The voxel-wise multiparametric fit was updated to perform a joint fit of SQ and TQ signal, using GlobalSearch and fmincon solver in Matlab (R2019a, Mathworks, Natick, MA, USA), providing T2*slow and T2*fast maps. In the occurrence of one aberrant T2* value, the signal fit was reverted to a mono-exponential decay (as in the case of pure saline). The cost function of the fit was implemented to weight the TQ signal first echoes higher than the later echoes and the SQ signal. The first echoes were chosen empirically to range from one to eleven to follow the characteristic curve of the TQ signal (see **Figure 1**) and to weight down the later echoes which have lower SNR (see Eq.[1-3]).

$$f_{fitTQ\_(i)(x)} = A_{TQ}\left(\exp\left(-\frac{TE}{T2s^*}\right) - \exp\left(-\frac{TE}{T2f^*}\right)\right)\exp\left(-\frac{\tau 1}{T2s^*}\right) + DC_{TQ};\ i = 1,2\ ^{(*)}$$

[1]

$$f_{fitSQ}(x) = \left(A_{SQ1}\exp\left(-\frac{TE+\tau 1+\tau 2}{T2s^*}\right) + A_{SQ2}\exp\left(-\frac{TE+\tau 1+\tau 2}{T2f^*}\right)\right)\exp\left(-\frac{TE+\tau 1+\tau 2}{T2s^*}\right) + DC_{SQ} \quad [2]$$

$$L2_{(x)} = \mathrm{w1} * \Sigma\left(\mathrm{TQ}_{\mathrm{data\ (TE\_1:TE\_11)}} - f_{\mathrm{fitTQ\_1}}(\mathrm{x})\right)^2 + \mathrm{w2} * \Sigma\left(\mathrm{TQ}_{\mathrm{data\ (TE\_12:TE\_21)}} - f_{\mathrm{fitTQ\_2}}(\mathrm{x})\right)^2 +$$

$$\mathrm{w2} * \Sigma\left(\mathrm{SQ}_{\mathrm{data}} - f_{\mathrm{fitSQ}}(\mathrm{x})\right)^2 \quad ^{(**)}\ [3]$$

<u>The variables in Eq. [1-3] are:</u>

A_{TQ} = triple quantum signal amplitude, A_{SQ1} = single quantum amplitude slow term, A_{SQ2} = single quantum amplitude fast term, $DC_{TQ,SQ}$ = DC offset to account for noise, TE = echo time, T2s* = T2*slow, T2f* = T2*fast, $\tau 1$= evolution time, $\tau 2$= mixing time.

$^{(*)}$ The TQ fit was split into two parts f_{fitTQ_1} and f_{fitTQ_2}: 1) data for echoes 1 to 11 that includes the expected TQmax signal and 2) data from echo 12 to the latest echo, after the expected TQmax signal, to allow for different weighting in the cost function L2.

$^{(**)}$ w1, w2 = weightings. The weightings were empirically optimized to w1=0.8 and w2=0.2. The fit routine included both T2*fast and T2*slow with boundary settings T2*fast: [2 ms; 10 ms] and T2*slow [8 ms; 55 ms].

175 *2.5 PHASE CYCLE OPTIMIZATION*

176 The phase increment of the chosen phase cycle was initially chosen with 30° to
177 conform to Nyquist criterion of sampling the signal along the phase axis with twice the
178 frequency of interest (i.e. 12 steps cycles). The minimum number of steps is 6 [1],
179 with corresponding phase increment of 60°, for the TQ acquisition and a decrease to
180 30° increment results in a 2-fold measurement time increase. As an optimization of
181 efficacy, 12-step ($\Delta\phi$ = 30°) datasets were subsampled into the 6-step subset of $\Delta\phi$
182 = 60° with the initial start phase of $\phi_1(t = 0) = 90°$. Additionally, two averages were
183 used to obtain higher SNR within allotted time. The initial 12-steps 2-averages results
184 were compared to the minimal 6-steps 1-average subset results in terms of SQ and
185 TQ SNR, both in vitro and in vivo.

186

187 *2.6 DATA EVALUATION*

188 We calculated the SNR of SQ and TQ along echo time within the whole image within
189 the 6-pixel eroded body mask and the standard deviation of the noise in the
190 background. Additionally, SNR was computed in the four 4 % and 5 % agar phantom
191 vials using centered circular regions of interest, 2 pixels smaller than the outline, to
192 avoid partial volume effects. The fit result contained T2*slow and T2*fast maps and
193 the fitted amplitudes for A_{SQslow}, A_{SQfast}, $A_{TQ.}$ The fit was performed for a single slice
194 chosen at the center of the 3D datasets, respectively.

195

196

197

3 RESULTS

3.1 PHANTOM RESULTS

The experimental results from 3D-CRISTINA with the phantom are given in **Figure 2** for the five central slices of each dataset. Compared to previous 2D results from [1], SNR dropped by 2.27 ± 0.46-fold with chosen acquisition parameters (**Supplementary Material Figure 1**). When correcting for the voxel size (5.21x5.21x20 mm^3 in 2D to 4x4x8 mm^3 in 3D), which led to a global SNR loss of 4.24-fold, the actual SNR gain for moving from 2D to 3D was 4.24/2.27 = 1.87-fold improvement. With 3D-CRISTINA, the three phantom vials: 2, 4, and 5, with an agar concentration of 4%, 4% and 5% can be clearly distinguished from the remaining vials on the TQ image. The relationship of TQ signal to agar concentration of the different > 40 mL vials, (vials 8,9 were not included due to their sizes) was linear with R^2 = 0.987 (**Figure 2 d,e**). The phantom vial 7 was disregarded due to the low sodium concentration leading to a limited SNR in SQ and TQ images.

3.2 FIT RESULTS

For the center slice, a multiparameter fit was performed (**Figure 3**) along echo time (**Equation 1-3**). The average T2* values were evaluated within each phantom vial and resulted in a mean $T2^*_{fast}$ and $T2^*_{slow}$ value of the phantom vials 2, 4, 5 and 8 which contained 4% and 5% of agarose, of ($T2^*_{fast}$: 5±2 ms; $T2^*_{slow}$: 34±9 ms). For vials 3, 6, and 9, which contained 2% agarose, we obtained: $T2^*_{fast}$: 8±3 ms; $T2^*_{slow}$: 50±5 ms. Vial 7 with 4% agar and 50 mM resulted in $T2^*_{fast}$ of 6±3 ms and $T2^*_{slow}$ of 44±15 ms. The liquid saline solution resulted in T2*: 34±11 ms.

3.3 PHASECYCLE OPTIMIZATION RESULTS

To virtually cut down measurement time by 4x (from 53 min to 13 min in vivo, and 64 min to 16 min in the phantom), we compared the initial 12-step phase cycle ($\Delta\phi$ = 30°) with two averages to a single cycle with $\Delta\phi$ = 60°. The comparison of SQ and TQ signals can be seen in **Figure 4** on phantom. By taking only a quarter of the data, the SQ SNR decreased by 39±5 % and the TQ SNR decreased by 31±2 %. The limited SNR drop (compared to expected 50 %) reflected the influence of samples position within the phase cycle. The extra 6 steps with initial phases 120°, 180°, 240°, 300° and 360° are not participating in the TQ signal build-up as they correspond to zero-crossing of the TQ signal. Additionally, these points contributed sub-optimally to SQ signal considering their relative amplitude in the SQ coherence profile, shaped by a sinus wave. **Figure 5** shows the results on in vivo data.

3.4 INVIVO HEALTHY VOLUNTEER RESULTS

Figure 6 showed the capacity of 3D-CRISTINAto visualize sodium SQ and TQ signals across the whole brain, even in regions of B0 inhomogeneity. TQ signal did not exhibit structured variations across slices, while SQ signal reflects the different concentrations of sodium between WM, GM and CSF. SQ results from the four healthy volunteers (**Figure 7)** showed consistent signal intensity distribution with conventional single pulse Na-MRI sequences [15]. From ROI measurements, mean TSC values showed an increase sodium concentration from WM to GM to CSF (52.9 ± 4.1, 96.6 ± 22.0 and 170.0 ± 23.9 mM respectively). Fitted signals TQ/SQ ratio exhibited a corresponding decrease from 0.28 ± 0.07 (WM) to 0.14 ± 0.04 (GM) and 0.10 ± 0.03 (CSF), reflecting a relatively homogeneous measured TQ signal in the whole brain. **Figure 7** showed TQ signal variations were much lower than SQ signal variations in all volunteers. Consequently, the TQ/SQ ratio showed strong differences between gray and white matter. White matter exhibited low SQ signal, levelled TQ

signal and thus higher TQ/SQ ratio, suggesting that despite a lower sodium concentration, a stronger bi-exponential signal separation derived from WM molecular environment. On the contrary, GM exhibited increased SQ signal from higher sodium concentrations, but TQ signal on the levels of WM. This relationship confirms a different balance of exponential components, with a larger component for the longer T2* decay [16]. Expectedly, CSF exhibited a negligible TQ/SQ ratio.

4 DISCUSSION

In this study, 3D-CRISTINA demonstrated consistent MQ images at 7T in a dedicated agar phantom. The non-selective excitation allowed to improve the spatial resolution and decrease the acquisition time, also combined with an increase in SNR. Furthermore, the choices for phase cycling were investigated and optimized retrospectively. The conservative phase cycling of 12 ($\Delta\phi = 30°$) steps was evaluated against 6 steps ($\Delta\phi = 60°$) options in the well-controlled phantom experiments. An acquisition time reduction from 66 min to 16.4 min in the phantom was possible without moderate SNR loss in the TQ signal. The phantom results motivated in vivo exploration in healthy volunteers in the brain where we found consistent results across slices and subjects. In vivo, total scan time reached 53 min for a whole brain coverage. The same 4-fold time reduction in vivo led to limited SNR loss, motivating the use of the 6-steps cycles only, with more averages if examination time permits it. Nevertheless, further developments could improve resulting SNR within limited time, utilizing multi-channels coil hardware and/or advanced image reconstruction techniques (compressed sensing or deep learning techniques [17]–[19]).

For tissue sodium concentration quantification in vivo, the SQ signal at the first echo time (TE_1=1 ms) was employed instead of the more accurate the fitted SQ signal at TE = 0 ms to avoid potential bias introduced by the bi-exponential fitting. Additionally, TSC references were defined by the CSF and the 100 mM vial instead of the 50 mM phantom vial for accuracy. Indeed, external vials placed at the edges of the coil might experience inhomogeneous B1+ that penalizes lower signal estimation.

The in vivo data exhibited a difference of TQ/SQ ratio between GM, WM and CSF in the four volunteers. Considering WM contains myelinated structured axons while GM is made up of cell bodies, the molecular environment of sodium atoms in these compartments is expected to strongly differ. However, CSF is expected to present a very low TQ/SQ ratio from relatively free molecular environment. Our results suggest current noise levels could bias proper estimation of very low TQ signal in CSF. Nevertheless, a larger study is warranted to confirm these initial results based on only four volunteers. Further study microstructure similar to Kolbe et al. [20] could be envisioned combining 3D-CRISTINA with DTI to map these differences in regard to the brain architecture.

One limitation of this study was the loss of SNR from too ambitious spatial resolution. The reduction of the voxel size was too drastic compared to the 1.87-fold SNR improvement provided by 3D-CRISTINA. A relatively lower resolution would have better shown 3D-CRISTINA benefits. Another limitation is the limited number of in vivo data for justified GM and WM quantification. An additional T1-weighted sequence (eg. the MP2RAGE sequence [21]) acquisition would have helped to provide a GM and WM segmentation. But the MP2RAGE sequence was designed to be employed with a multi-channel receiver coil array, requiring a change of coil which was incompatible with this study [22]. Another clear limitation is the low SQ and TQ signal of phantom vial 7 (4 % agar and 50 mM ^{23}Na), further work is needed with

297 standardized fabricated phantoms to explore limitations and rule out phantom ageing
298 problems.
299 Further, signal variations in TQ images need to be explored to rule out variations due
300 to B1+ field inhomogeneities. With our current coil, we measured flip angles deviation
301 up to 10% within in the brain, which remains an acceptable precision. In addition, a
302 comparison of healthy volunteers to pathological indications is necessary to evaluate
303 the sensitivity of the TQ signal obtained by this sequence.
304 We reported an updated processing routine that is jointly fitting the SQ and TQ data
305 to obtain T2* fast and slow parameters. We chose to weigh down the later TQ signal
306 after TE>15ms in the loss function. The earlier part (TE<15ms) contains the
307 characteristic curve and should be more accurate in the determination of T2* values.
308 Nevertheless, it must be emphasized that the cost function weights were chosen
309 empirically. The reported T2* values align with the literature [13]. We limited our
310 conclusions for in vivo exploration based on TQ, SQ signals and their ratio, which are
311 more consistent measures for tissue characterization than the higher complexity
312 CRISTINA model.
313
314 While 2D-CRISTINA focused on phase cycling schemes and probing multi-quantum
315 pathways with accuracy and efficacy, 3D-CRISTINA considers practical MRI
316 acquisition towards in vivo sodium multi-quantum imaging. In this study, we explored
317 the feasibility of CRISTINA in the whole brain at 7T. Next, further work towards the
318 more readily available clinical field strength of 3T is also warranted for more
319 accessible multi-quantum imaging. This could extend the current state of the art in
320 sodium imaging that relies up to date on the single quantum imaging for tissue sodium
321 characterization with ultrashort echo time sequences [23], [24].
322

In conclusion, the presented technological advances enabled consistent sodium MQC imaging in acceptable time for research investigations, which offers the possibility to study ionic distribution and environment in neuropathologies such as multiple sclerosis, stroke or tissue degradation after radiation therapy in dedicated protocols. [25] This step is important for the active research field of ^{23}Na imaging which is especially interested in the biochemical characterization of tissue.

LIST OF FIGURE CAPTIONS

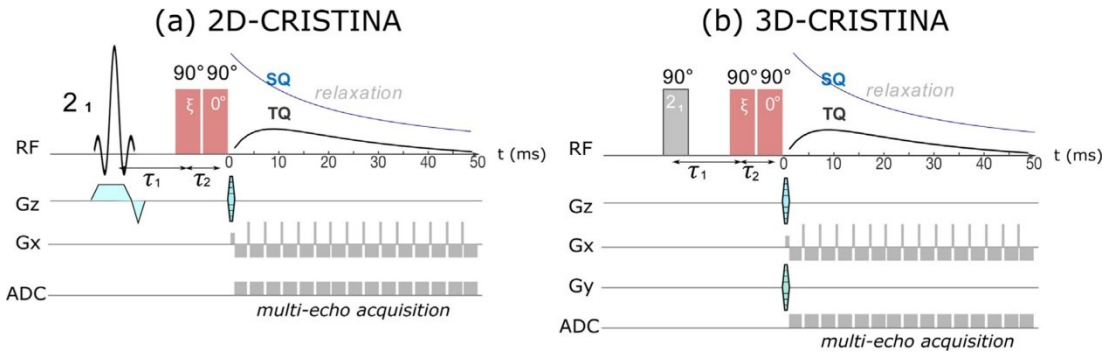

Figure 1: The previous 2D-CRISTINA sequence (a) featuring three pulses for multi-quantum excitation, was extended to 3D-CRISTINA (b) by adding an additional phase encoding direction and substituting the slice selection by a non-selective excitation.

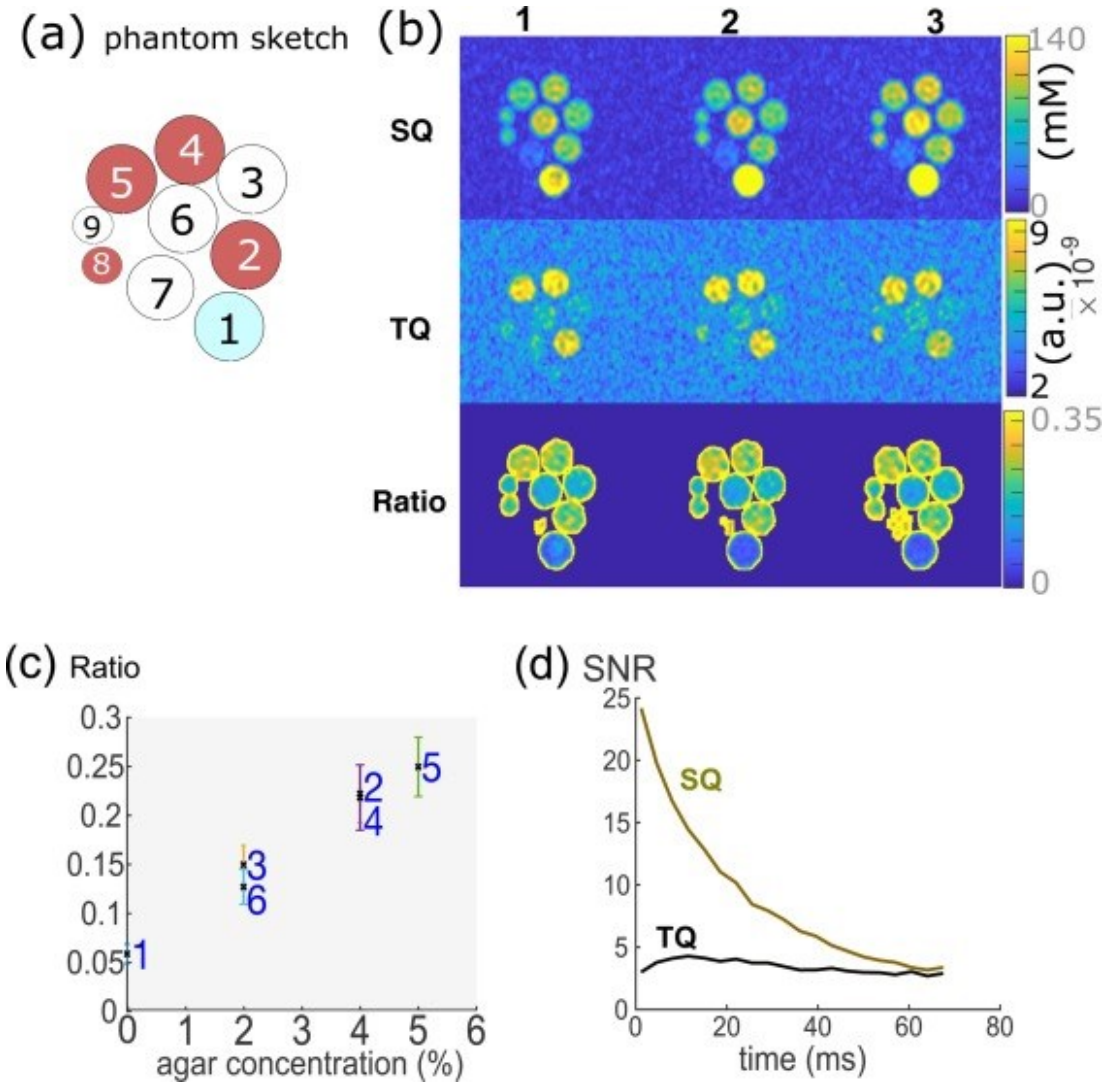

Figure 2: (a) Phantom design for subsequent sequence evaluation composed of nine tubes with different agar (in %) and sodium concentration (in mM): 1) 0 %, 154 mM, 2) 4 %, 100 mM 3) 2 % agar, 100 mM 4) 4 %, 154 mM 5) 5 %, 154 mM 6) 2 % 130 mM 7) 4 % 50 mM 8) 4 % 100 mM 9) 2 %, 100 mM. Phantom vial 8 and 9 have a much smaller volume with 14 mL compared to the 2-5 with 40 mL. The phantom vials indicated in red correspond to the high agar vials containing >4 % agar. b) Phantom result of 3D-CRISTINA, SQ and TQ signal and their ratio for 3 central slices each. (c) For the ratio versus agar concentration evaluation without phantom 7-9 the result was: R2 = 0.987, p = 6e-5. (d) The SNR of TQ and SQ over echo time shows the characteristic signal evolution respectively.

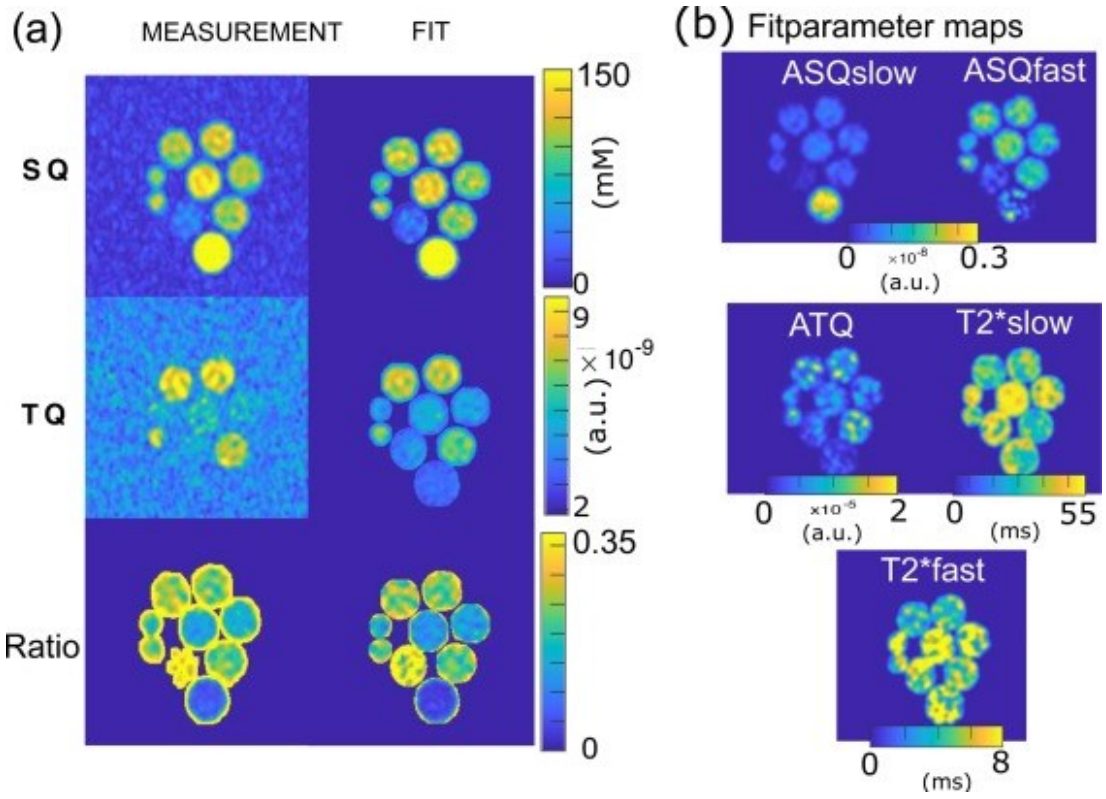

345

346 **Figure 3:** Fit result for the phantom dataset for a single slice at the center of the dataset. (a)
347 results with the measurement and fit data side by side. The fit was performed only within the
348 body mask therefore the Fit results and Ratios are zero in the background. (b) Resulting fit
349 parameter maps corresponding to Eq. 1-3. The liquid vial follows a mono-exponential decay
350 by comparing the signal amplitudes ASQslow and ASQfast maps. In the T2* maps it can be
351 appreciated that the higher agarose phantoms show shorter relaxation times.

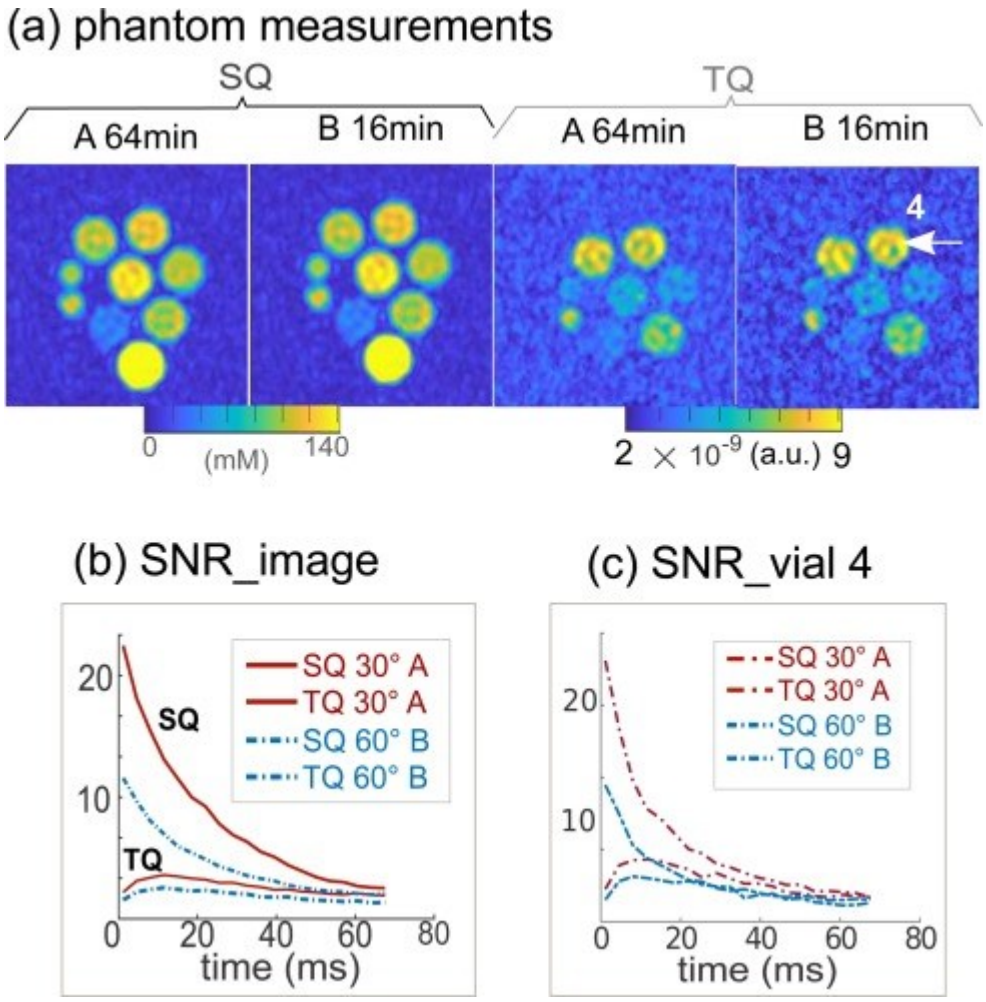

Figure 4: (a) phantom measurement comparison of TQ and SQ signal when doubling the phase cycle increment. (A) 64min was acquired with a phase cycle increment of $\Delta\phi$ = 30° and two cycles of each 6 steps. For (B) 16min, the increment was doubled to $\Delta\phi$ = 60°, without averaging, acquiring only a fourth of the data. The SQ and TQ SNR for the whole image was evaluated in (b). Due to cutting the amount of data the SNR is higher for A than for B, however visibly the image quality is not compromised, confirming the possibility of a shorter measurement time. (c) the SNR in vial 4 shows the signal comparison for A versus B measurement time in the 4 % 154 mM vial.

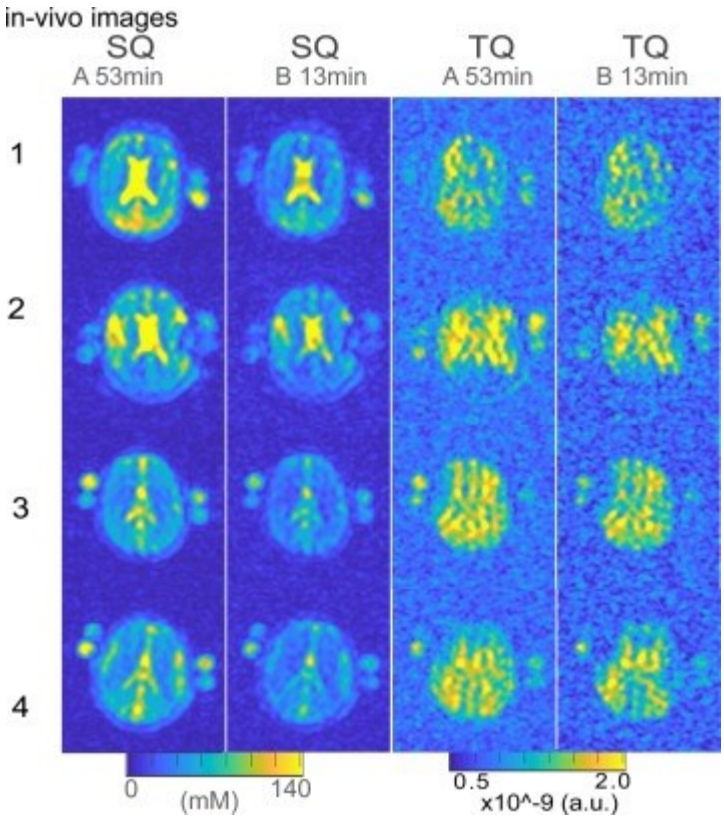

361

362 **Figure 5:** Visual Comparison of TQ and SQ signal when doubling the phase cycle increment,
363 without averaging, in vivo for the 4 different healthy volunteers in analogy to the phantom
364 measurement shown in Figure 4.

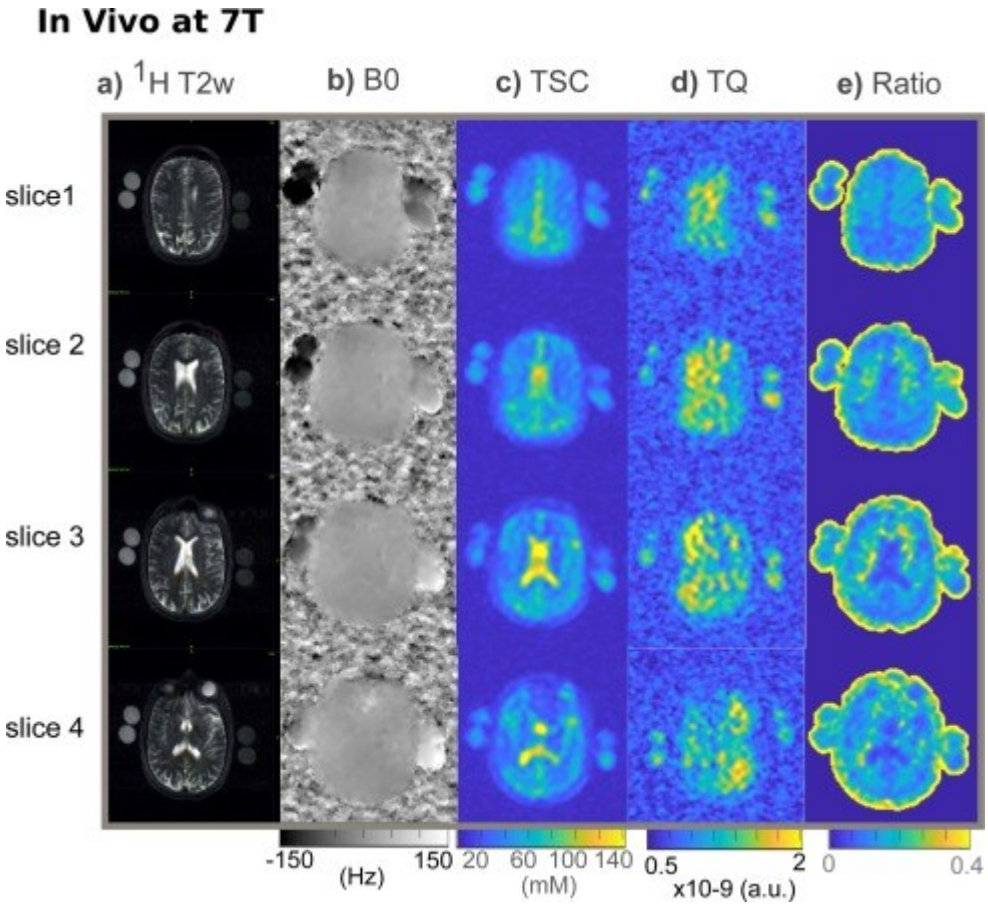

Figure 6: 7T in vivo results, different slices of volunteer 1. (A) T2w transversal ^{1}H image showing the corresponding slices. (B,C) ^{1}H-T2w overlay with SQ and TQ signal to relate the high intensity regions to the morphology better described by ^{1}H images. (D) B0 maps reconstructed from the multi-echo CRISTINA data, (E) SQ images quantified to Tissue Sodium Concentration, (F) TQ images as well as the ratio of SQ and TQ signal in (G).

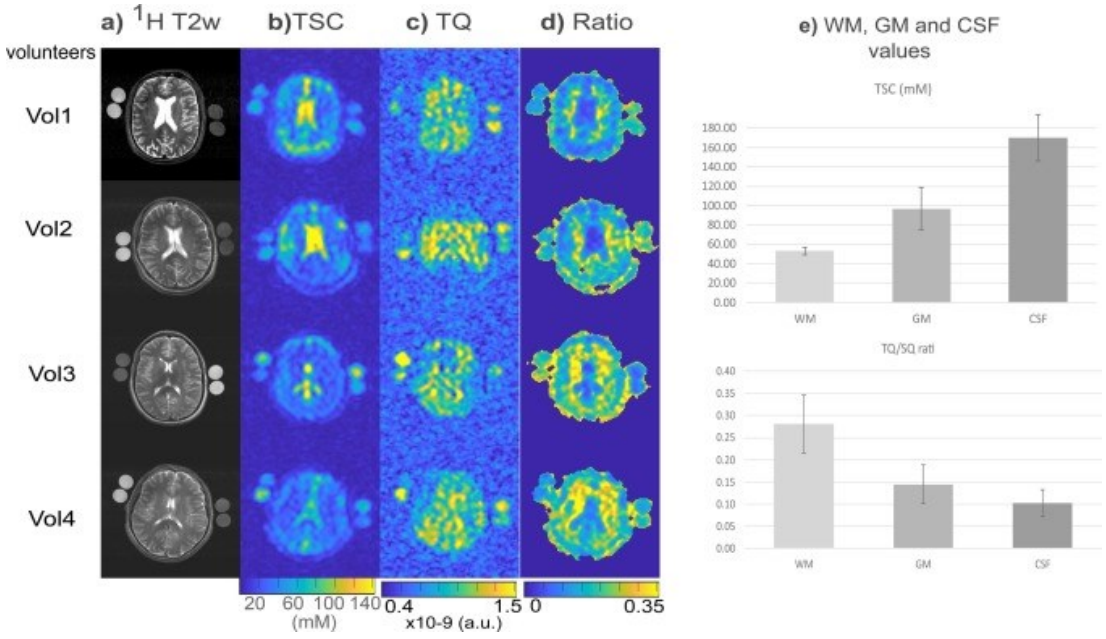

371

372 **Figure 7:** 7T in vivo results of the four volunteers demonstrated homogeneous TQ signal
373 within the brain, with occasional darker regions in the periphery. These signal losses might be
374 associated with the extra B1 sensitivity of TQ signal (to the power of 5). Interestingly, the
375 TQ/SQ ratio highlighted regions of white matter in all volunteers, and low ratio values in
376 cerebro-spinal fluid area.

377

378

Acknowledgements

This work was performed by a laboratory member of France Life Imaging network (grant ANR-11-INBS-0006), on the platform 7T-AMI, a French “Investissements d’Avenir” programme” (grant ANR-11-EQPX-0001). This work was supported by the Excellence Initiative of Aix-Marseille University - A*MIDEX, a French “Investissements d’Avenir” programme (grant A*MIDEX-EI-17-29-170228-09.43-Imetionic-7), Aix-Marseille Université, AP-HM and CNRS (Centre National de la Recherche Scientifique). This work was supported by the “Förderprogramm” MEAMEDMA of the medical faculty Mannheim.

The authors would like to thank Claire Costes, Lauriane Pini, Patrick Viout and Véronique Gimenez for their support in this study.

REFERENCES

[1] M. A. U. Hoesl, L. R. Schad, and S. Rapacchi, “Efficient 23Na triple-quantum signal imaging on clinical scanners: Cartesian imaging of single and triple-quantum 23Na (CRISTINA),” *Magn Reson Med*, vol. 84, no. 5, pp 2412-2428, Nov. 2020

[2] S. Romanzetti, C. C. Mirkes, D. P. Fiege, A. Celik, J. Felder, and N. J. Shah, “Mapping tissue sodium concentration in the human brain: A comparison of MR sequences at 9.4Tesla,” *Neuroimage*, vol. 96, pp. 44–53, Aug. 2014.

[3] K. R. Thulborn, “Quantitative sodium MR imaging: A review of its evolving role in medicine,” *Neuroimage*, vol. 168, pp. 250–268, Mar. 2018.

[4] D. Wagner, M. Anton, and H. Vorwerk, “Dose uncertainty in radiotherapy of patients with head and neck cancer measured by in vivo ESR/alanine dosimetry using a mouthpiece.,” *Phys. Med. Biol.*, vol. 56, no. 5, pp. 1373–83, 2011.

[5] R. Hu, D. Kleimaier, M. Malzacher, M. A. U. Hoesl, N. K. Paschke, and L. R. Schad, “X-nuclei imaging: Current state, technical challenges, and future directions,” *J. Magn. Reson. Imaging*, vol. 0, no. 0, May 2019.

[6] K. Huhn, T. Engelhorn, R. A. Linker, and A. M. Nagel, “Potential of Sodium MRI as a Biomarker for Neurodegeneration and Neuroinflammation in Multiple Sclerosis ,” *Frontiers in Neurology* , vol. 10. p. 84, 2019.

[7] K. R. Thulborn, D. Davis, J. Snyder, H. Yonas, and A. Kassam, “Sodium MR Imaging of Acute and Subacute Stroke for Assessment of Tissue Viability,” *Neuroimaging Clin. N. Am.*, vol. 15, no. 3, pp. 639–653, Aug. 2005.

[8] M. Bydder *et al.*, “Dynamic 23Na MRI - A non-invasive window on neuroglial-vascular mechanisms underlying brain function,” *Neuroimage*, vol. 184, pp. 771–780, 2019.

[9] M. Inglese *et al.*, “Brain tissue sodium concentration in multiple sclerosis: A sodium imaging study at 3 tesla,” *Brain*, vol. 133, no. 3, pp. 847–857, 2010.

[10] G. Madelin and R. R. Regatte, “Biomedical applications of sodium MRI in vivo,” *J. Magn. Reson. Imaging*, vol. 38, no. 3, pp. 511–529, 2013.

[11] G. Bodenhausen, H. Kogler, and R. R. Ernst, “Selection of coherence-transfer pathways in NMR pulse experiments,” *J. Magn. Reson.*, vol. 58, no. 3, pp. 370–388, 1984.

[12] R. Pohmann, O. Speck, and K. Scheffler, “Signal-to-noise ratio and MR tissue parameters in human brain imaging at 3, 7, and 9.4 tesla using current receive coil arrays,” *Magn. Reson. Med.*, vol. 75, no. 2, pp. 801–809, Feb. 2016.

[13] G. Madelin, J. S. Lee, R. R. Regatte, and A. Jerschow, “Sodium MRI: Methods and applications,” *Prog. Nucl. Magn. Reson. Spectrosc.*, vol. 79, pp. 14–47, 2014.

[14] L. Fleysher, N. Oesingmann, and M. Inglese, “B0 inhomogeneity-insensitive triple-quantum-filtered sodium imaging using a 12-step phase-cycling scheme,” *NMR Biomed.*, vol. 23, no. 10, pp. 1191–1198, Dec. 2010.

[15] N. J. Shah, W. A. Worthoff, and K.-J. J. Langen, “Imaging of sodium in the brain: A brief review,” *NMR Biomed.*, vol. 29, no. 2, pp. 162–174, Feb. 2016.

[16] B. Ridley *et al.*, “Distribution of brain sodium long and short relaxation times

and concentrations: a multi-echo ultra-high field 23Na MRI study," *Sci. Rep.*, vol. 8, no. 1, pp. 1–12, 2018.

[17] M. Lustig and D. Donoho, "Compressed sensing MRI," *Signal Process. …*, vol. 25, no. 2, pp. 72–82, 2008.

[18] F. A. Breuer *et al.*, "Controlled aliasing in volumetric parallel imaging (2D CAIPIRINHA)," *Magn. Reson. Med.*, vol. 55, no. 3, pp. 549–556, 2006.

[19] F. A. Breuer, M. Blaimer, R. M. Heidemann, M. F. Mueller, M. A. Griswold, and P. M. Jakob, "Controlled aliasing in parallel imaging results in higher acceleration (CAIPIRINHA) for multi-slice imaging," *Magn. Reson. Med.*, vol. 53, no. 3, pp. 684–691, 2005.

[20] S. C. Kolbe *et al.*, "Microstructural correlates of 23Na relaxation in human brain at 7Tesla," *Neuroimage*, vol. 211, no. February, p. 116609, 2020.

[21] U.-S. Choi, H. Kawaguchi, Y. Matsuoka, T. Kober, and I. Kida, "Brain tissue segmentation based on MP2RAGE multi-contrast images in 7T MRI," *PLoS One*, vol. 14, no. 2, pp. e0210803–e0210803, Feb. 2019.

[22] S. Lachner *et al.*, "Comparison of optimized intensity correction methods for 23Na MRI of the human brain using a 32-channel phased array coil at 7Tesla," *Z. Med. Phys.*, vol. 30, no. 2, pp. 104–115, 2020.

[23] A. M. Nagel, F. B. Laun, M. A. Weber, C. Matthies, W. Semmler, and L. R. Schad, "Sodium MRI using a density-adapted 3D radial acquisition technique," *Magn. Reson. Med.*, vol. 62, no. 6, pp. 1565–1573, 2009.

[24] Y. Qian and F. E. Boada, "Acquisition-weighted stack of spirals for fast high-resolution three-dimensional ultra-short echo time MR imaging," *Magn.*

Reson. Med., vol. 60, no. 1, pp. 135–145, Jul. 2008.

[25] S. A. Mohamed *et al.*, “MRI Detection of Changes in Tissue Sodium Concentration in Brain Metastases after Stereotactic Radiosurgery: A Feasibility Study,” *J. Neuroimaging*, vol. 31, no. 2, pp. 297-305 Mar. 2021.